



HAL
open science

micro-RNA 21 detection with a limit of 2 pM in 1 min using a size-accordable concentration module operated by electrohydrodynamic actuation

Inga Tijunelyte, Rémi Malbec, Bayan Chami, Jean Cacheux, Christophe Dez, Thierry Leichlé, Pierre Cordelier, Aurélien Bancaud

► To cite this version:

Inga Tijunelyte, Rémi Malbec, Bayan Chami, Jean Cacheux, Christophe Dez, et al.. micro-RNA 21 detection with a limit of 2 pM in 1 min using a size-accordable concentration module operated by electrohydrodynamic actuation. *Biosensors and Bioelectronics*, 2021, 178, pp.112992. 10.1016/j.bios.2021.112992 . hal-03449104

HAL Id: hal-03449104

<https://cnrs.hal.science/hal-03449104v1>

Submitted on 26 Nov 2021

HAL is a multi-disciplinary open access archive for the deposit and dissemination of scientific research documents, whether they are published or not. The documents may come from teaching and research institutions in France or abroad, or from public or private research centers.

L'archive ouverte pluridisciplinaire **HAL**, est destinée au dépôt et à la diffusion de documents scientifiques de niveau recherche, publiés ou non, émanant des établissements d'enseignement et de recherche français ou étrangers, des laboratoires publics ou privés.

micro-RNA 21 detection with a limit of 2 pM in one minute using a size-accordable concentration module operated by electrohydrodynamic actuation

Inga Tijunelyte¹, Rémi Malbec¹, Bayan Chami¹, Jean Cacheux¹, Christophe Dez², Thierry Leichlé^{1,3}, Pierre Cordelier⁴, Aurélien Bancaud^{1,*}

AFFILIATION

¹ CNRS, LAAS, 7 avenue du colonel Roche, F-31400, Toulouse, France.

² Laboratoire de Biologie Moléculaire Eucaryote (LBME), Centre de Biologie Intégrative (CBI), Université de Toulouse, CNRS, UPS, F-31062, Toulouse, France

³ GeorgiaTech-CNRS Joint International Laboratory, School of Electrical and Computer Engineering, Atlanta, GA, USA

⁴ Université Fédérale de Toulouse Midi-Pyrénées, Université Toulouse III Paul Sabatier, CRCT, Toulouse, France

*Correspondance : abancaud@laas.fr; LAAS-CNRS, 7 avenue du colonel Roche BP 54200 31031 Toulouse cedex 4, France

ABSTRACT

We present a fluorimetry-based technology for micro-RNA-21 (miR-21) sensing based on the concentration of miR-molecular beacon (MB) complexes and flushing of unbound MB. This concentration module consists of a microfluidic channel with the shape of a funnel operated with electrohydrodynamic actuation. We report a limit of detection of 2 pM in less than one minute for miR-21 alone, and then demonstrate that miR-21 levels measured in fine needle biopsy samples from patients with pancreatic cancer correlate with the reference technique of reverse-transcription polymerase chain reaction (RT-PCR). Altogether, this technology has promising clinical performances for the follow-up of patients with cancer.

KEYWORDS

Electrohydrodynamic migration, RNA/DNA concentration, miR-21, fine needle biopsy

1 Introduction

MicroRNAs (miRs) are single-stranded RNA molecules of 15–27 nucleotides that regulate gene expression at the post-translational level. miR concentration is profoundly altered in cancer, and this deregulation may participate to carcinogenesis (Calin and Croce, 2006; Pichler and Calin, 2015). Monitoring miRs levels thus constitutes a valuable prospect for the management of patients with cancer (Etheridge et al., 2011). Next-generation sequencing, which provides genome-wide miR expression levels, is essential for *de novo* identification of miR-based biomarkers. Yet, the processing of clinical samples, which contain very low material input, remains a challenge (Coenen-Stass et al., 2018). For targeted miRs quantification, the gold standard is Reverse-Transcriptase quantitative Polymerase Chain Reaction (RT-qPCR) and its miniaturized low background version (RT-digital droplet PCR, ddPCR; (Forero et al., 2019)), which rely on labor intensive protocols with multiple controls (Stein et al., 2017).

Alternatively, the race for fast technologies that do not rely on enzymatic amplification has not slowed down (Cacheux et al., 2019). Enzyme-free technologies for miR titration can coarsely be cast into two categories depending on whether detection occurs in bulk or on surfaces. Surface detection reaches high sensitivity but generally depends on sophisticated microfabrication strategies (Ansari et al., 2016). Bulk detection is readily achieved by fluorimetry, and most frequently relies on molecular beacons (MBs), which change conformation and become fluorescent upon hybridization to the target (Baker et al., 2011). This method is limited in sensitivity to 1 nM (Baker et al., 2011) and dynamic range due to the background signal from unreacted MBs (Garcia-Schwarz and Santiago, 2012). The limit of detection (LOD) has nevertheless been decreased to the fM level by replacing organic fluorophores with quantum dots (Su et al., 2014), or to 5 pM using more sophisticated signal transduction schemes based on endonucleases that provoke the release of a fluorophore engrafted to the probe and initially quenched by a gold nanoparticle (Degliangeli et al., 2014). Furthermore, signal amplification schemes based on strand displacement reactions have been implemented in order to convert each miR hybridization event into a cascade of detectable readouts (Li et al., 2015; Wu et al., 2015). These assays reached sub-pM to sub-fM LODs (Liang et al., 2017; Song et al., 2016; Wang et al., 2019; Wu et al., 2016), though at the expense of generally long time to result (Shin et al., 2019).

In another yet non-mutually exclusive direction, fast and sensitive detection characterized by a LOD of 5 pM in 3 minutes has been reported by concentrating miR-MB complexes with isotachopheresis (Bahga et al., 2013; Bercovici et al., 2012; Persat and Santiago, 2011). Concentration can also be performed with the μ -Laboratory for DNA analysis and separation (μ LAS) technology, which is based on the combination of hydrodynamic transport and a counter electrophoretic force (Malbec et al., 2019; Milon et al., 2020; Ranchon et al., 2016). Electrohydrodynamic actuation induces transverse migration oriented toward the channel walls. Because transverse forces increase with hydrodynamic flow velocity, electrophoretic velocity, and DNA molecular weight (MW) (Chami et al., 2020, 2018), this technology enables DNA separation in a linear channel, *i.e.* with constant hydrodynamic and electrophoretic settings. In a microchannel with the shape of a funnel, the amplitude of transverse forces progressively increases as the flow velocity and electric field build up near the constriction (Fig. 1A). By adjusting the pressure and tension, hydrodynamic and electrophoretic forces (along the x-axis in Fig. 1A) can be balanced to define a position of null velocity. Upstream of this stagnation point, hydrodynamic forces prevail so that molecules continuously flow to and accumulate at this position. Here, we use μ LAS for detection of the cancer-promoting miR-21 (Humeau et al., 2015; Pfeffer et al., 2015) based on the selective enrichment of miR-21:MB complexes and elimination of unbound MB due to their lower MW. In “ideal” conditions, *i.e.* with a mixture only containing the MB and miR-21, we report a LOD of 2 pM within 30 seconds. We then prove that miR-21 titration can be performed in complex samples containing high concentrations of uncomplimentary RNA, and establish that absolute miR-21 levels measured in fine-needle biopsy samples of patients with pancreatic cancer are correlated to those of RT-qPCR.

2 Materials and methods

2.1 Microfluidic chips and data acquisition

Microfluidic chips were fabricated following the same protocol as described in ((Malbec et al., 2019), see Supplementary Material). The maximal and minimal channel widths were 800 and

5 μm , respectively, and its depth at the constriction was 2 μm (Fig. 1A). The chip was filled with a solution containing 22 mM of NaCl and 5% (m:v) 1.3 MDa polyvinylpyrrolidone (the viscosity and relaxation time of the solution were 31 mPa.s and 1.1 ms, respectively (Naillon et al., 2019)). Actuation was operated using a 7 bar pressure controller (Fluigent) and a DC high voltage power supply (Labsmith). Videos were recorded with a Leica microscope equipped with a light engine for cyan excitation (Lumencore) and an sCMOS digital camera (Hamamatsu). We used a 20X air objective (Numerical Aperture of 0.8) and 4x4 binning (pixels of 1.3 μm). The inter-frame interval was set to 2 s with an exposure time of 0.2 s.

2.2 Fine needle biopsy samples

Fine needle biopsy material was obtained from the Bacap repository (The BACAP Consortium et al., 2018). Total RNA was extracted with miRNeasy Micro Kit (Qiagen). For miR reverse transcription, we used 10 ng of total RNA and miRCURY™ LNA™ miRNA RT Kit (Qiagen). Real-time PCR for miR-21 was performed using LNA™-enhanced microRNA qPCR primers (Qiagen) and the StepOne plus sequence detection system (Applied Biosystems).

2.3 Genomic sequences

miR-21C: 5'-(A)₃₅-TAGCTTATCAGACTGATGTTGA-(A)₃₅-3'.

miR-21: 5'-UAGCUUAUCAGACUGAUGUUGA-3'

MB: 5'-FAM-GCGCGTCAACATCAGTCTGATAAGCTACGCGC-BHQ1-3', FAM, and BHQ1 standing for 6-carboxyfluorescein and black-hole quencher 1.

3 Results and discussion

3.1 Electrohydrodynamic actuation settings for miR-21 detection

We first report the analysis of a stoichiometric solution of the miR-21 target (miR-21C) and a complementary MB at 100 nM in the microfluidic chip of 2 μm in height (Fig. 1A). We used a pressure of 2.5 bar and a counter electrophoretic force associated to a tension of 275 V. The resulting maximum flow velocity v_0^{max} and electric field E^{max} were 20 mm/s and 17

kV/cm, respectively (see definition in Fig. 1A and details of the calculation in Supplementary Material). The corresponding Reynolds number and electrophoretic Peclet number were 10^{-3} and 50, respectively, implying that the flow was laminar and electrophoresis occurred. We confirmed that the electric field did not induce temperature change, and that electrohydrodynamic actuation did not impair nucleic acid pairing (Supplementary Fig. S1). In Fig. 1B, we plot miR-21C:MB concentration kinetics. Within few seconds after application of the electric field, a fluorescence signal became measurable at the constriction (image 1 in Fig. 1B). The fluorescence intensity signal, as inferred from a Gaussian fit of the intensity signal along the symmetry axis of the chip (inset of Fig. 1B and red dashed arrow in the upper right micrograph), reached a plateau after ~40 s. As soon as the electric field was turned off, trapped molecules were flushed out from the concentrator (image 4), and the fluorescence signal dropped back to its initial level. These concentration and flush cycles could be repeated multiple times with a repeatability of ~10% for consecutive experiments on the same chip and 25% in between different chips (Supplementary Fig. S2). Notably, in comparison to a fragment of 1 kbp (Milon et al., 2020), the concentration of the miR-21C:MB complex of ~30 bp required flow velocities and electric fields enhanced by 20-fold and 200-fold, respectively.

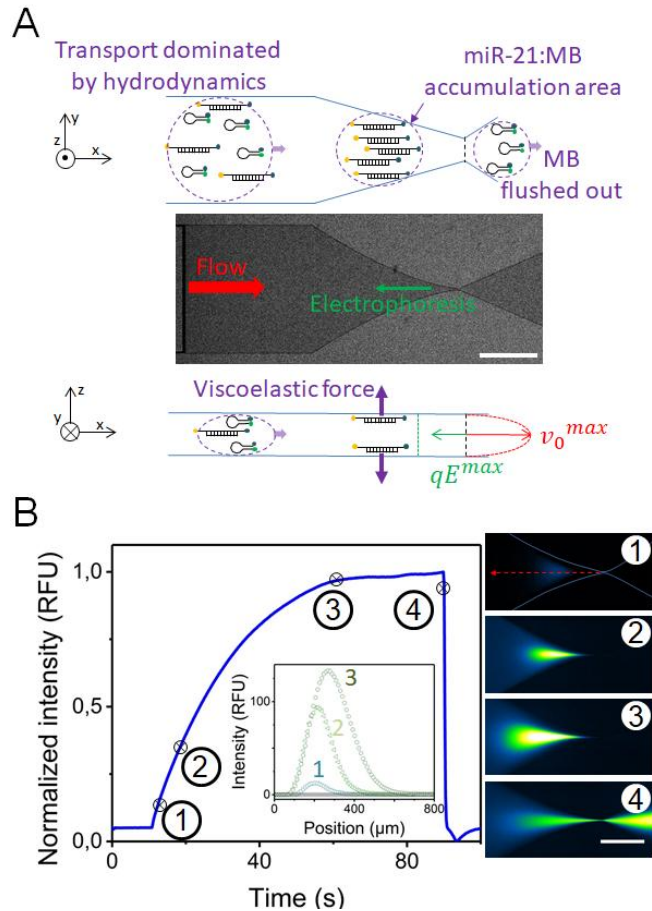


Figure 1. μ LAS technology for miR-21 sensing. (A) The panel shows a sketch and an optical micrograph of the microfluidic chip. The hydrodynamic flow field is oriented toward the funnel and electrophoretic forces in the counter-flow direction. The flow velocity and electric field are maximal at the tip of the apex. Viscoelastic forces are controlled by electrohydrodynamic settings, and adjusted to concentrate miR-21:MB complexes and flush unbound MB (linear and hairpin structures, respectively). (B) The graph shows the temporal evolution of the maximum fluorescence intensity in relative fluorescence units (RFU), as deduced from the peak of the intensity profile along the symmetry axis of the channel (plot in inset). Numbers in fluorescence micrographs correspond to highlighted points in the graph. The scale bar corresponds to 100 μ m.

3.2 Selective concentration of miR-21:MB complex

To prove the selective concentration of the miR:MB complex and concomitantly the flushing of unbound MB, we performed one experiment with a “dual chip” containing two

funnels in tandem operated with the same electrohydrodynamic settings, as initially designed for sizing expanded alleles in neurodegenerative diseases ((Malbec et al., 2019), micrographs in Fig. 2A). This chip geometry allowed us to directly and instantaneously compare two mixtures composed of miR-21C and MB at concentrations of 1 and 100 nM or 10 and 100 nM (blue and black datasets in Fig. 2A, respectively). After one minute of concentration using v_0^{max} and E^{max} of 30 mm/s and 19 kV/cm, a strong and a faint signal were observed in the channels that coincided with the difference in miR-21C concentration (micrograph 1 in Fig. 2A). The ratio of the two signals of ~ 9.2 fold in fact nearly matched the 10-fold difference in solution concentration. As the electric field E^{max} was increased to 24 kV/cm, we noted that concentrated miR-21C:MB complexes migrated in the counter-flow direction associated to a drop of the signal at the constriction (See supplementary Movie 1 and Fig. 2A). This response was readily explained by the build-up of electrophoretic forces that triggered a mode of transport dominated by electrophoresis. Then, the fluorescence signal at the constriction started to increase again with the same intensity in both channels. This even signal corresponded to the residual fluorescence of unbound MB, which are concentrated at higher electric fields due to their low MW. Consequently, this experiment showed that MB or miR-21C:MB could be selectively concentrated by tuning electrohydrodynamic settings. Interestingly, the concentration pattern of unbound MB resembled that of a “moustache” (image 2 in Fig. 2A). This shape could readily be accounted for by the insufficient electric field to efficiently concentrate MB, as already described in (Arca et al., 2016), and the difference between electric and hydrodynamic field profiles near the boundaries. Electrophoresis prevailed near the lateral walls, because the fluid flow field decreased more rapidly than the electric field (Stone et al., 2004). Conversely, the electric field was insufficient to stop molecules at the symmetry axis of the channel, where hydrodynamic forces were maximal. The resulting pattern of depletion at the center and accumulation at the walls was that of a moustache.

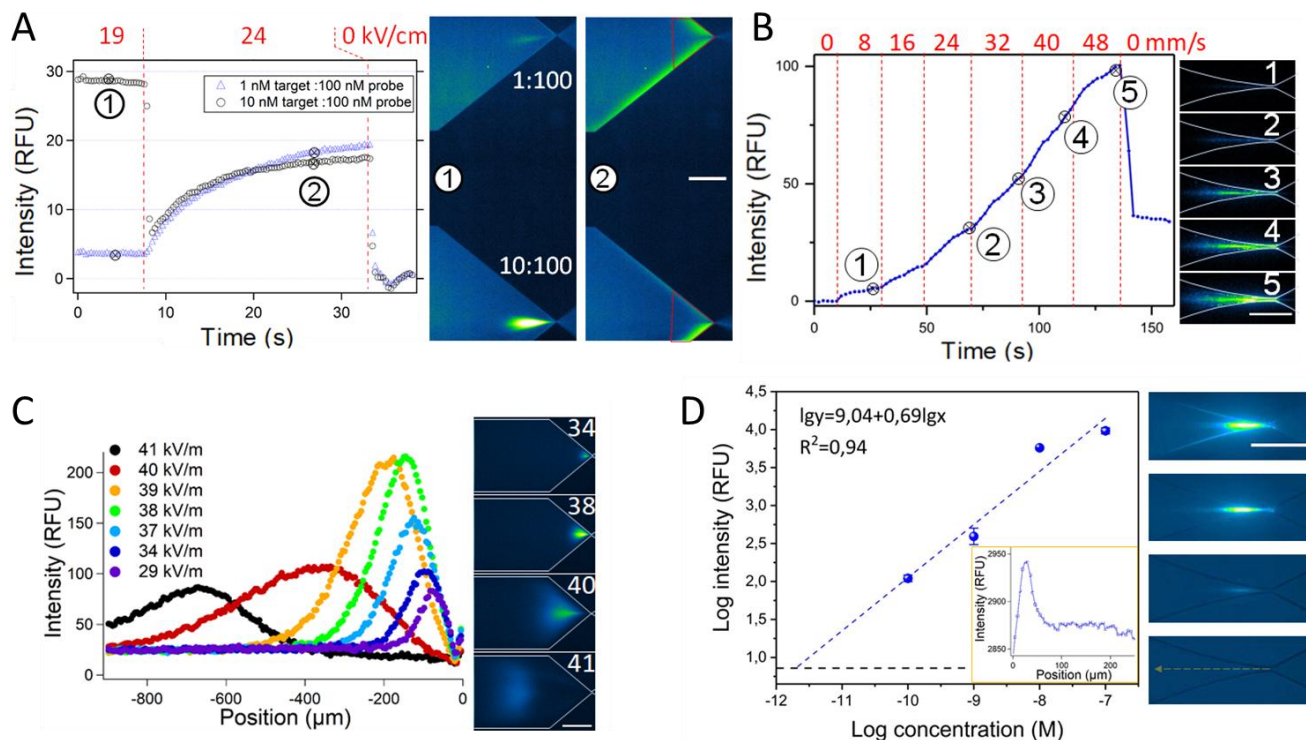


Figure 2. Detection of miR-21 in ideal conditions. (A) The blue and black datasets represent the signal over time in each channel of the dual chip. The first 15 s correspond to the steady concentration pattern of miR-21:C:MB at E^{\max} and v_0^{\max} of 19 kV/cm and 30 mm/s. The electric field is then increased to 24 kV/cm, and the intensity becomes comparable in both channels. The electric field is eventually turned off to flush the chip. (B) The graph shows the temporal variation of the peak fluorescence intensity using a stoichiometric miR-21-C:MB concentration of 100 nM. E^{\max} is set to 9.4 kV/cm and v_0^{\max} spans 0 to 48 mm/s, as indicated in the upper red panel. Numbers in fluorescence micrographs correspond to highlighted numbers in the graph. (C) The plot presents the fluorescence intensity profile along the symmetry axis of the channel. Experiment is performed with stoichiometric miR-21:C:MB concentrations of 100 nM, v_0^{\max} is set to 7 cm/s, and E^{\max} ranges from 0 to 41 kV/cm. The four micrographs at the right are recorded at 34, 38, 40, 41 kV/cm after 20 s of concentration. (D) The graph on the left shows miR-21:MB fluorescence signal as a function of miR-21 nominal concentration. MB concentration, E^{\max} and v_0^{\max} are set to 100 nM, 15 kV/cm, and 16 mm/s, respectively. The plot in inset presents the intensity profile along the symmetry axis of the channel for 0.1 nM of miR-21. The four micrographs correspond to concentrations of miR-21 of 100, 10, 1, and 0.1 nM (from top to bottom). The scale bars represent 200 μm .

3.3 Detection of miR-21 with a LOD of 2 pM in 30 s

We subsequently aimed to optimize electrohydrodynamic actuation settings to enhance miR-21C:MB signal. First, using a constant electric field E^{max} of 9.4 kV/cm, we increased the pressure by steps of 1 bar, each lasting 20 s, *i.e.* v_0^{max} increased from 8 to 48 mm/s (upper red indications in Fig. 2B). This experiment showed a succession of linear regimes for the concentration kinetics, the first five slopes being roughly proportional to the flow rate (not shown). Hence, hydrodynamics expectedly constituted the source of convection to the concentration module, implying that high flow rates were beneficial to detection. We then performed a “mirror” experiment where v_0^{max} was set to 70 mm/s and E^{max} gradually increased from 29 to 41 kV/cm (Fig. 2C, see Supplementary Fig. S3 for the temporal variation of the signal). The maximum of the intensity profile along the symmetry axis of the channel increased with E^{max} from 29 to 38 kV/cm, and the position of the peak shifted away from the constriction (Fig. 2C). The maximum intensity signal then dropped, showing that the modulation of the electric field was critical to obtain peaked miR-21:MB signals. Given that we could not apply more than 200 V without a high risk of damaging the chip due to oxide breakdown, optimal detection therefore consisted in increasing the flow rate to obtain the highest signal to noise ratio for a tension of 200 V.

We finally focused on miR-21 detection by preparing four mixtures with 100 nM of MB and miR-21 at concentrations spanning 0.1 to 100 nM. The samples were consecutively analyzed in one chip starting from the lowest miR-21 concentration. We set v_0^{max} and E^{max} to 16 mm/s and 15 kV/cm (these conditions were consistent with ones used for fine needle biopsy samples, see below). The miR-21:MB fluorescence signal was inferred from the peak of the intensity plot along the symmetry axis of the channel, as shown in the inset of Fig. 2D. The saturation of the signal occurred after 30 s for the four samples (Supplementary Fig. S4). The signal of 110 and the standard deviation of the noise of 4.3 were associated to a signal to noise ratio of 25 for the lowest miR-21 concentration of 0.1 nM (inset of Fig. 2D). We then estimated the LOD by plotting the signal as a function of miR-21 nominal concentration (Fig. 2D). The power-law response associated to an exponent of 0.7 could be extrapolated to a signal equal to two times the

standard deviation of the background (Nič et al., 2009), leading to a LOD of 2.0 pM. Notably, the comparison of different MB batches showed an unexplained variability in miR-21:MB fluorescence signal, which was characterized by different power-law scaling signatures but comparable LODs (Supplementary Fig. S5).

3.4 miR-21 detection in fine needle biopsy samples

miR-21 detection in biological samples is challenging because large amounts of background RNA molecules with broad size distributions are present in the sample (see the size distribution of the RNA extracted from pancreas cancer cell lines in Supplementary Fig. S6). We thus aimed to investigate whether and how background RNA molecules could affect the detection capabilities of our technology. For this, we reconstituted two “model” mixtures using (i) one RNA ladder with 7 bands of 100 to 1000 nt, and (ii) total RNA extracted from yeast cell cultures, which predominantly contained two bands of 1800 and 3400 nt. These solutions were diluted in buffer at a final concentration of 5 ng/ μ L, *i.e.* a comparable concentration to that of fine needle biopsy samples (see below), and they were spiked with 1, 10, and 100 nM miR-21 with the MB at 100 nM. We also prepared control solutions without RNA background, and processed the resulting nine samples on the same chip. In Fig. 3A, we report the fluorescence signal at constant E^{max} of 9.4 kV/cm and varying v_0^{max} from 4 to 32 mm/s. In the control, fluorescence intensity increased linearly with pressure, whereas a plateau was reached in both reconstituted samples for v_0^{max} greater than 16 mm/s (see micrographs in Supplementary Fig. S7). At v_0^{max} of 12 mm/s (Fig. 3B), we noticed that the power law exponent relating the signal to miR-21 concentration remained in the same range of 0.5 to 0.7 with or without RNA background. Moreover, although slightly degraded to 3 pM with the yeast RNA background, the LOD remained very comparable in the three samples. Hence, we performed miR-21 titration experiments in five fine needle biopsy samples from patients with pancreatic cancer in the low pressure regime with v_0^{max} and E^{max} of 12 mm/s and 9.4 kV/cm. After determination of the total RNA concentration by absorbance spectroscopy, ranging from 150 to 400 ng/ μ L, we diluted the samples down to the same total RNA concentration of \sim 20 ng/ μ L (see values in the inset of Fig. 3C). The associated miR-21 levels spanned nearly two decades from 3 to 260 pM. The five samples were processed in

one chip, and the total time of analysis was ~ 120 minutes with five consecutive detection cycles of 1 minute followed by rinsing during 15 minutes. We obtained a detectable signal for the five samples, and the plot of miR-21 fluorescence signal as a function of miR-21 nominal concentration measured by RT-qPCR showed a correlation associated to a coefficient of 0.7 (Fig. 3C). Note that the signal of the negative control (MB alone, red line in Fig. 3C) recorded at the end of experiment was lower than the signal for every patient sample. Though refined measurements over a larger cohort would clarify the discrepancy between the reference of RT-qPCR and our data for some samples, especially the samples with a RT-qPCR concentration of 100 and 3 pM, we concluded that miR-21 titration can be operated in clinical samples.

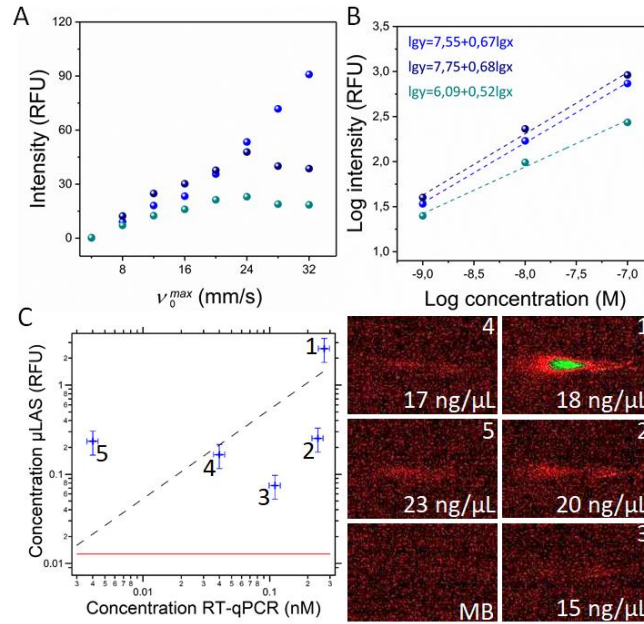


Figure 3: Detection of miR-21 in complex samples. (A) The plot presents fluorescence intensity as a function of v_0^{\max} at constant E^{\max} of 9.4 kV/cm using stoichiometric miR-21:MB concentration of 100 nM without background or with 5 ng/ μL of low range RNA ladder or yeast total RNA (light blue, dark blue, or green dataset, respectively). (B) The plot shows miR-21:MB fluorescence signal as a function of miR-21 concentration for v_0^{\max} and E^{\max} 12 mm/s and 9.4 kV/cm. The color code of the datasets is the same as in (A). (C) The plot presents miR-21 intensity signal as a function of miR-21 concentration inferred from RT-qPCR for v_0^{\max} and E^{\max} of 12 mm/s and 9.4 kV/cm. MB concentration is 50 nM, and its analysis alone yields the signal plotted with the red horizontal line. The micrographs present the fluorescence intensity patterns (note that the signal before actuation is subtracted for clarity). **The scale bar corresponds to 100 μm .**

4 Conclusions

In summary, an enzyme-free miR sensing strategy based on the selective concentration of miR hybridized to MB has been established. The LOD of 2 pM in one minute outperforms conventional MB bulk detection, and compares well to other concentration-based high sensitivity miR biosensing technologies. Further, we proved that the simplicity and rapidity of this technology was relevant to measure miR-21 levels in fine needle biopsy patients' samples. In order to enhance the sensitivity of this technology, two synergetic and complementary developments can be envisioned. First, the concentration module performances can be improved by optimizing the microfluidic chip geometry. Second, strand displacement reactions to amplify the readout signal can be integrated ahead of the microfluidic concentration module in the detection process.

Declaration of interest:

The authors declare that they have no known competing financial interests or personal relationships that have appeared to influence the work in this paper.

CRedit authorship contribution statement:

Inga Tijunelyte: Conceptualization, Investigation, Data curation, writing. **Rémi Malbec:** Conceptualization, Investigation. **Bayan Chami:** Investigation, writing, editing. **Jean Cacheux:** Investigation. **Christophe Dez:** Investigation, **Thierry Leichlé:** Supervision, editing. **Pierre Cordelier:** Supervision, clinical study management, editing. **Aurélien Bancaud:** Supervision, conceptualization, writing, funding acquisition.

Acknowledgments:

The authors thank Moinamina Mze Ahmed for help in the experiments with fine needle biopsy samples, and Yves Dusabyinema for BioAnalyzer RNA analysis. This work was partly supported by the LAAS-CNRS micro and nanotechnologies platform, member of the French RENATECH network. R.M. and B.C. thank the Carnot institute and Ligue contre le Cancer, respectively, for their PhD fellowships, and J.C. for the funding of the 4th year of PhD by Fondation ARC. This project was partly supported by the ANR μ LAS (ANR-16-CE18-0028-01) and the ANR Biopulse (ANR-16-ASTR-0020). The authors wish to thank the members of the BACAP consortium. BACAP consortium: 1 Barbara Bournet, Cindy Canivet, Louis Buscail, Nicolas carrère, Fabrice Muscari, Bertrand Suc, Rosine Guimbaud, Corinne Couteau, Marion Deslandres, Pascale Rivera, Anne-Pascale Laurenty, Nadim Fares, Etienne Buscail, Karl Barange, Janick Selves, Anne Gomez-Brouchet. 2 Bertrand Napoléon, Bertrand Pujol, Fabien Fumex, Jérôme Desrame, Christine Lefort, Vincent Lepilliez, Rodica Gincul, Pascal Artru, Léa Clavel, Anne-Isabelle Lemaistre. 3 Laurent Palazzo; 4 Jérôme Cros; 5 Sarah Tubiana; 6 Nicolas Flori, Pierre Senesse, Pierre-Emmanuel Colombo, Emmanuelle Samail-Scalzi, Fabienne Portales, Sophie Gourguou, Claire Honfo Ga, Carine Plassot, Julien Fraisse, Frédéric Bibeau, Marc Ychou; 7 Pierre Guibert, Christelle de la Fouchardière, Matthieu Sarabi, Patrice Peyrat, Séverine Tabone-Eglinger, Caroline Renard; 8 Guillaume Piessen, Stéphanie Truant, Alain Saudemont, Guillaume Millet, Florence Renaud, Emmanuelle Leteurtre, Patrick Gele; 9 Eric Assenat, Jean-Michel Fabre, François-Régis Souche, Marie Dupuy, Anne-Marie Gorce-Dupuy, Jeanne Ramos; 10 Jean-

François Seitz, Jean Hardwigsen, Emmanuelle Norguet-Monnereau, Philippe Grandval, Muriel Duluc, Dominique Figarella-Branger; 11 Véronique Vendrely, Clément Subtil, Eric Terrebonne, Jean-Frédéric Blanc, Jean-Philippe Merlio; 12 Dominique Farges-Bancel, Jean-Marc Gornet, Daniela Geromin; 13 Geoffroy Vanbiervliet, Anne-Claire Frin, Delphine Ouvrier, Marie-Christine Saint-Paul; 14 Philippe Berthelémy, Chelbabi Fouad; 15 Stéphane Garcia, Nathalie Lesavre, Mohamed Gasmi, Marc Barthet; 16 Vanessa Cottet; 17 Cyrille Delpierre.

1 The CHU and the University of Toulouse, Toulouse, France; 2 Jean Mermoz Hospital, Ramsay Général de Santé, Lyon, France; 3 Trocadéro Clinic, Paris, France; 4 The Department of Pathology, Beaujon Hospital and Paris 7 University, Clichy, France.5 The Biobank, Bichat Hospital and Paris 7 University, Paris, France; 6 The Cancer Institute and the University of Montpellier, Montpellier, France; 7 The Léon Bérard Cancer Center, Lyon, France;8 The Department of Digestive Surgery, the CHU and the University of Lille, Lille, France;9 The CHU and the University of Montpellier, Montpellier, France.10 La Timone Hospital and the University of Marseille, Marseille, France;11 The CHU and the University of Bordeaux, Bordeaux, France;12 Saint Louis Hospital and Paris 7 Diderot University, Paris, France;13 The CHU and the University of Nice, Nice, France;14 Pau Hospital, Pau, France;15 The CHU Nord Hospital and the University of Marseille, Marseille, France;16 INSERM UMR866 and the University of Dijon, Dijon, France;17 INSERM UMR1027 and the University of Toulouse, Toulouse France.

References

- Ansari, M.I.H., Hassan, S., Qurashi, A., Khanday, F.A., 2016. *Biosens. Bioelectron.* 85, 247–260. <https://doi.org/10.1016/j.bios.2016.05.009>
- Arca, M., Ladd, A.J., Butler, J.E., 2016. *Soft Matter* 12, 6975–6984.
- Bahga, S.S., Han, C.M., Santiago, J.G., 2013. *I The Analyst* 138, 87–90. <https://doi.org/10.1039/C2AN36249J>
- Baker, M.B., Bao, G., Searles, C.D., 2011. *INucleic Acids Res.* gkr1016. <https://doi.org/10.1093/nar/gkr1016>
- Bercovici, M., Han, C.M., Liao, J.C., Santiago, J.G., 2012. *Proc. Natl. Acad. Sci.* 109, 11127–11132. <https://doi.org/10.1073/pnas.1205004109>
- Cacheux, J., Bancaud, A., Leichlé, T., Cordelier, P., 2019. *Front. Chem.* 7, 815. <https://doi.org/10.3389/fchem.2019.00815>
- Calin, G.A., Croce, C.M., 2006. *Nat. Rev. Cancer* 6.

- Chami, B., Milon, N., Fuentes Rojas, J.-L., Charlot, S., Marrot, J.-C., Bancaud, A., 2020. *Talanta* 217, 121013. <https://doi.org/10.1016/j.talanta.2020.121013>
- Chami, B., Socol, M., Manghi, M., Bancaud, A., 2018. *Soft Matter* 14, 5069–5079. <https://doi.org/10.1039/c8sm00611c>
- Coenen-Stass, A.M.L., Magen, I., Brooks, T., Ben-Dov, I.Z., Greensmith, L., Hornstein, E., Fratta, P., 2018. *ERNA Biol.* 15, 1133–1145. <https://doi.org/10.1080/15476286.2018.1514236>
- Degliangeli, F., Kshirsagar, P., Brunetti, V., Pompa, P.P., Fiammengo, R., 2014. *Absolute and Direct J. Am. Chem. Soc.* 136, 2264–2267. <https://doi.org/10.1021/ja412152x>
- Etheridge, A., Lee, I., Hood, L., Galas, D., Wang, K., 2011. *Mutat. Res. Mol. Mech. Mutagen., MicroRNA in Environmental Mutagenesis* 717, 85–90. <https://doi.org/10.1016/j.mrfmmm.2011.03.004>
- Forero, D.A., González-Giraldo, Y., Castro-Vega, L.J., Barreto, G.E., 2019. *BioTechniques* 67, 192–199. <https://doi.org/10.2144/btn-2019-0065>
- Garcia-Schwarz, G., Santiago, J.G., 2012. *Anal. Chem.* 84, 6366–6369. <https://doi.org/10.1021/ac301586q>
- Humeau, M., Vignolle-Vidoni, A., Sicard, F., Martins, F., Bournet, B., Buscail, L., Torrisani, J., Cordelier, P., 2015. *PLoS ONE* 10, e0130996. <https://doi.org/10.1371/journal.pone.0130996>
- Li, W., Jiang, W., Ding, Y., Wang, L., 2015. *Biosens. Bioelectron.* 71, 401–406. <https://doi.org/10.1016/j.bios.2015.04.067>
- Liang, C.-P., Ma, P.-Q., Liu, H., Guo, X., Yin, B.-C., Ye, B.-C., 2017. *Angew. Chem. Int. Ed.* 56, 9077–9081. <https://doi.org/10.1002/anie.201704147>
- Malbec, R., Chami, B., Aeschbach, L., Ruiz Buendía, G.A., Socol, M., Joseph, P., Leichlé, T., Trofimenko, E., Bancaud, A., Dion, V., 2019. *Sci. Rep.* 9, 23. <https://doi.org/10.1038/s41598-018-36632-5>
- Milon, N., Fuentes Rojas, J.-L., Castinel, A., Bigot, L., Bouwmans, G., Baudelle, K., Boutonnet, A., Gibert, A., Bouchez, O., Donnadieu, C., Ginot, F., Bancaud, A., 2020. *Lab. Chip* 20, 175–184. <https://doi.org/10.1039/c9lc00965e>
- Naillon, A., de Loubens, C., Chèvremont, W., Rouze, S., Leonetti, M., Bodiguel, H., 2019. *Phys. Rev. Fluids* 4, 053301. <https://doi.org/10.1103/PhysRevFluids.4.053301>
- Nič, M., Jiráť, J., Košata, B., Jenkins, A., McNaught, A. (Eds.), 2009. *IUPAC Compendium of Chemical Terminology: Gold Book, 2.1.0.* ed. IUPAC, Research Triangle Park, NC. <https://doi.org/10.1351/goldbook>
- Persat, A., Santiago, J.G., 2011. *Anal. Chem.* 83, 2310–2316. <https://doi.org/10.1021/ac103225c>
- Pfeffer, S.R., Yang, C.H., Pfeffer, L.M., 2015. *Drug Dev. Res.* 76, 270–277. <https://doi.org/10.1002/ddr.21257>
- Pichler, M., Calin, G.A., 2015. *Br. J. Cancer* 113, 569–573. <https://doi.org/10.1038/bjc.2015.253>
- Ranchon, H., Malbec, R., Picot, V., Boutonnet, A., Terrapanich, P., Joseph, P., Leichlé, T., Bancaud, A., 2016. *Lab. Chip* 16, 1243–1253. <https://doi.org/10.1039/c5lc01465d>
- Shin, S.W., Ahn, S.Y., Lim, Y.T., Um, S.H., 2019. *Anal. Chem.* 91, 14808–14811. <https://doi.org/10.1021/acs.analchem.9b03173>
- Song, C.Y., Yang, Y.J., Yang, B.Y., Sun, Y.Z., Zhao, Y.P., Wang, L.H., 2016. *Nanoscale* 8, 17365–17373. <https://doi.org/10.1039/C6NR05504D>
- Stein, E.V., Duewer, D.L., Farkas, N., Romsos, E.L., Wang, L., Cole, K.D., 2017. *PloS One* 12, e0188085. <https://doi.org/10.1371/journal.pone.0188085>
- Stone, H.A., Stroock, A.D., Ajdari, A., 2004. *Annu Rev Fluid Mech* 36, 381–411.

- Su, S., Fan, J., Xue, B., Yuwen, L., Liu, X., Pan, D., Fan, C., Wang, L., 2014. *ACS Appl. Mater. Interfaces* 6, 1152–1157. <https://doi.org/10.1021/am404811j>
- The BACAP Consortium, Canivet, C., Gourgou-Bourgade, S., Napoléon, B., Palazzo, L., Flori, N., Guibert, P., Piessen, G., Farges-Bancel, D., Seitz, J.-F., Assenat, E., Vendrely, V., Truant, S., Vanbiervliet, G., Berthelémy, P., Garcia, S., Gomez-Brouchet, A., Buscail, L., Bournet, B., 2018. *BMC Cancer* 18, 986. <https://doi.org/10.1186/s12885-018-4906-4>
- Wang, Ganglin, Yu, M., Wang, Guoping, 2019. *Biosens. Bioelectron.* 138, 111319. <https://doi.org/10.1016/j.bios.2019.111319>
- Wu, H., Liu, Y., Wang, H., Wu, J., Zhu, F., Zou, P., 2016. *Biosens. Bioelectron.* 81, 303–308. <https://doi.org/10.1016/j.bios.2016.03.013>
- Wu, Z., Liu, G.-Q., Yang, X.-L., Jiang, J.-H., 2015. *J. Am. Chem. Soc.* 137, 6829–6836. <https://doi.org/10.1021/jacs.5b01778>